Supplementary Materials for Length-Variable Bionic Continuum Robot With Millimeter-Scale Diameter and Compliant Driving Force

Shiying Zhao, Qingxin Meng, *Member, IEEE*, Xuzhi Lai, Jinhua She, *Fellow, IEEE*, Edwardo Fumihiko Fukushima, *Member, IEEE*, and Min Wu, *Fellow, IEEE*

I. Customization of Backbone Stiffness

In the robot structure design, the backbone stiffness is an important parameter that needs to be considered. With low stiffness, the backbone is easy to buckle when the backbone length is varied. Besides, if the stiffness is too high, the backbone deflection is low, and the deformation ability of the backbone is limited. Therefore, it is necessary to choose the appropriate backbone stiffness to balance the buckling resistance and the deformation ability.

For our designed CR, the stiffness of the polyimide hollow tubes in the backbone is almost negligible compared to the central elastic rod. Therefore, the backbone stiffness is mainly determined by the central elastic rod. In this paper, we select three central rods with different stiffness: stainless steel rod, Nitinol rod (the elastic rod adopted in this paper), and polyether ether ketone (PEEK) rod. The length of each rod is 150 mm. The diameter of the stainless steel rod and the Nitinol rod is 0.5 mm. Due to the low stiffness of the PEEK rod, it is difficult to maintain a straight state with a diameter of 0.5 mm, which is not conducive to the buckling resistance test. Thus, we choose a PEEK rod with a diameter of 1 mm.

These rods are respectively fixed on a base and placed on the electronic balance, as shown in Fig. S1(A)-S1(C). Apply horizontal downward force to the rod endpoint until the endpoint reaches "12 cm" of a ruler to simulate the buckling situation, and the numbers of the electronic balance for each rod are shown in Fig. S1(D)-S1(F), which are 38.73 g, 26.37 g, and 15.42 g respectively. The larger the number, the greater the buckling resistance of the backbone made of the corresponding material. According to Fig. S1(D)-S1(F), the stainless steel rod, which exhibits the highest stiffness, is the least susceptible to buckling. Conversely, the PEEK rod, which displays the lowest stiffness, is the most prone to buckling, despite its largest diameter. The performance of the Nitinol rod falls somewhere between these two situations.

In addition, the deformation ability of the three rods is also verified. To simulate the bending deformation of the CR, we fix three magnetic spacer disks on each rod. One end of a cable is tied to the side hole of the bottom disk in each rod, and the other end passes through the side holes of the other two disks, connected to a tension gauge. Hold the tension gauge and pull the cable so that the endpoint of each rod reaches the position of "12 cm" in a ruler. The numbers of the tension gauge are shown in Fig. S1(G)-S1(I), which are 1.39 N, 0.96 N, and 0.24 N respectively. The larger the number, the poorer the deformation ability of the rod. It can be found that the deformation ability of the PEEK rod is the strongest, and that of the stainless steel rod is the worst. The performance of the Nitinol rod is also somewhere in between.

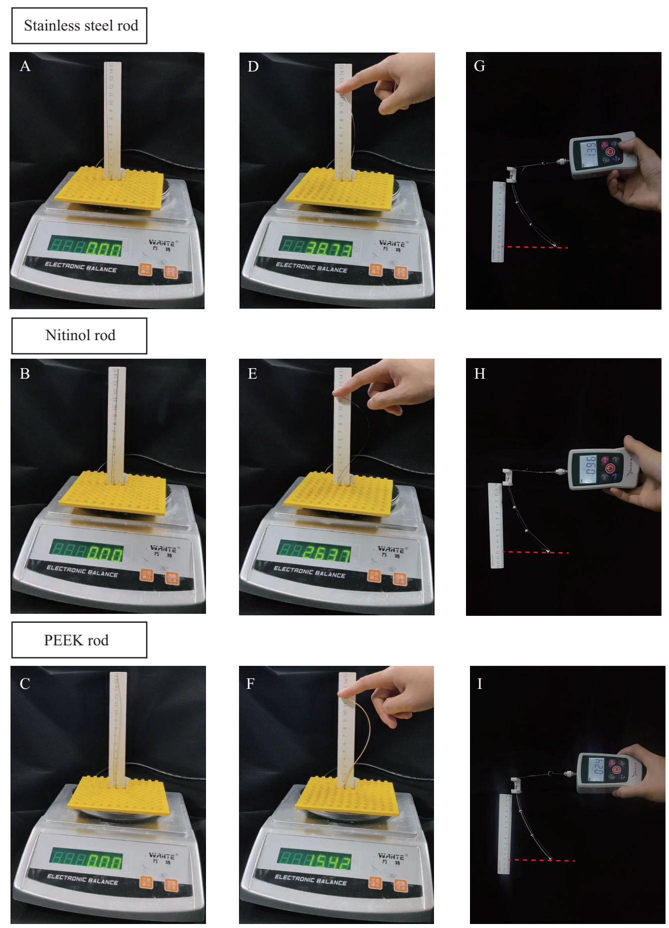

Fig. S1 Buckling resistance and deformation ability of different central rods. (A) Initial state of stainless steel rod. (B) Initial state of Nitinol rod. (C) Initial state of PEEK rod. (D) Number of electronic balance for stainless steel rod. (E) Number of electronic balance for Nitinol rod. (F) Number of electronic balance for PEEK rod. (G) Number of tension gauge for stainless steel rod. (H) Number of tension gauge for Nitinol rod. (I) Number of tension gauge for PEEK rod.

According to the above experiments, the Nitinol rod with moderate stiffness has not only a certain buckling resistance, but also a good deformation ability. Additionally, the Nitinol rod exhibits superelastic properties compared to the stainless steel rod, allowing it to restore its initial shape even after multiple large deformations. In contrast, the stainless steel rod undergoes a certain degree of plastic deformation after repeated significant bending, which reduces the operational lifespan of the designed robot. Therefore, we choose the Nitinol rod as the center elastic rod for the backbone in our designed CR.

II. Parameters and Fabrication of Robot Body

To quantify the size of the robot body designed in this paper, the specific values of the geometric symbols in Fig. 2 for the robot body are listed in Table S-I.

Fabricating a complete robot body involves the following steps: 1) Absorb an iron sheet with a special-shaped magnet, and adjust the alignment angle to form a magnetic spacer disk with three side holes and a central hole (Fig. S2(A)). Repeat the above process eighteen times to obtain all the magnetic spacer disks required for a robot body. 2) Insert the elastic rod into the polyimide hollow tube 3 and glue them together (Fig. S2(B)), prepare six magnetic spacer disks, and stick one to the end of the polyimide hollow tube 3 by the glue (Fig. S2(C)). The remaining five magnetic spacer disks are automatically mutually exclusive on the polyimide hollow tube 3 (Fig. S2(D)). 3) Prepare 6 magnetic spacer disks, stick one to the end of the polyimide hollow tube 2 (Fig. S2(E)), and arrange the remaining five mutually exclusive magnetic spacer disks on the polyimide hollow tube 2. 4) Prepare 6 magnetic spacer disks, stick one to the end of the polyimide hollow tube 1 (Fig. S2(F)), and make the rest five magnetic spacer disks arrange automatically. In this way, we have all the components of the backbone (Fig. S2(G)). 5) Assemble the products of the steps 2)-4), tie three cables to the three side holes of the glued magnetic spacer disk in each segment, and make the cables pass through the subsequent magnetic spacer disks. (Fig. S2(H)). 6) Stick the ends of the three polyimide hollow tubes with the three stainless steel tubes (Fig. S2(I)).

It should be noted that from segment 3 to segment 1, the cable number passed through the side holes increases in turn. To avoid the tying and winding of the cables, especially in segment 1, when designing and using the robot system, the following measures are considered. First of all, the design of the magnetic spacer disk allows the sizes of the side holes to be adjusted according to the cable number. This ensures that the area of the side holes is minimized while preventing the cables from getting stuck. Consequently, the relative movements of the multiple cables are restricted, effectively preventing the tying and winding of the cables, as illustrated in Fig. S3(A). In the overall design of the robot, a configuration of multiple magnetic spacer disks with moderate distance between the adjacent disks is employed. Furthermore, when the designed CR deforms, the soft drives coordinate with each other, ensuring that each cable remains tensioned. This operational method, combined with the configuration of multiple magnetic spacer disks, effectively prevents the relative movements of the cables in the side holes, thereby avoiding tying and winding issues, as illustrated in Fig. S3(B).

III. Parameters and Fabrication of Soft Drives

The specific parameters of the soft drives in Fig. 3 are shown in Table S-II.

The fabrication of the soft drive with large PSA and that of the soft drive with small PSA are similar. Here, we take the soft drive with large PSA as the object to show its fabricating steps: 1) Obtain a silicone tube by injection molding technology (Fig. S4(A)). 2) Cover the silicone tube with a fiber-reinforced layer to limit its unnecessary radial expansion (Fig. S4(B)). 3) Insert plug A and plug B coated with the glue into both sides of the silicone tube (Fig. S4(C) and Fig. S4(D)). The difference between the plug A and plug B is that the plug B has a hole to inflate and deflate the silicone tube. The silicone tube, fiber-reinforced layer and plugs make up the PSA. 4) Embed the plug B in the fixed side (Fig. S4(E)). 5) Insert the plug A into the moving side (Fig. S4(F)). The whole soft drive with large PSA is shown in Fig. S4(G).

IV. Pneumatic Platform

The pneumatic platform is composed of a computer (CPU: AMD Ryzen 7 3700X; Memory: 16G; Manufacturer: Lenovo; Sampling time: 0.01 s), an I/O module (Model number: PCI-1727U; Manufacturer: ADVANTECH), an air compressor (Model number: ES18L; Manufacturer: Eluan; Volume: 18 L), and twelve proportional-pressure regulators (Model number: VPPI-5L-3-G18-1V1H-V1-S1D; Manufacturer: Festo; Output pressure range: -1∼1 bar). Its block diagram is shown in Fig. S5.

The computer calculates the control pressures $P_{cn}(n = 1, 2, \ldots, 12)$ of the robot system according to the control method. It should be noted that, the twelve proportional-pressure regulators are driven by analog voltages. Thus, the computer converts the control pressures $P_{cn}(n = 1, 2, \ldots, 12)$ into the analog voltage signals $V_n(n = 1, 2, \ldots, 12)$, which are sent to the proportional-pressure regulators through the I/O module. Here, $V_n = P_{cn}/\alpha + \beta$. $\alpha = 0.2$ is the proportional coefficient for the proportional-pressure regulators, and $\beta = 5$ is the bias voltage. Subsequently, the proportional-pressure regulators adjust the inner pressures of the robot system according to $V_n(n = 1, 2, \ldots, 12)$ under the support of the air source from the air compressor. Generally, the proportional-pressure regulators can make the inner pressures of the robot system match their control pressures.

V. Characteristic Analysis Platform

The characteristic analysis platform is used to analyze the pressure-displacement and pressure-force characteristics of two groups of soft drives. The schematic diagram of the sensors and soft drives is shown in Fig. S6.

Fig. S6(A) and Fig. S6(B) are used to analyze the pressure-displacement characteristics for two groups of soft drives. One side in each group of soft drives is restricted by a fixed trestle, and the other side can move freely under the

Table S-1 Parameters of Robot Body

Symbol	Definition	Value
r	Cutting depth	0.5 mm
d	Cutting width	1 mm
Φ, φ	Central hole diameters	1.5 mm
D, γ	Outer diameters of special-shaped magnet and iron sheet	6 mm
q	Spacing angle	120°
t, f	Thicknesses of special-shaped magnet and iron sheet	2 mm and 1 mm
w	Large hole width	0.8 mm
h	Small hole width	0.5 mm
Δ	Diameter of fixed area	4 mm
λ_1	Inner diameter of polyimide hollow tube 3	0.54 mm
λ_2	Outer diameter of polyimide hollow tube 3	0.6 mm
λ_3	Inner diameter of polyimide hollow tube 2	0.94 mm
λ_4	Outer diameter of polyimide hollow tube 2	1 mm
λ_5	Inner diameter of polyimide hollow tube 1	1.12 mm
λ_6	Outer diameter of polyimide hollow tube 1	1.2 mm
C_1	Elastic rod diameter	0.5 mm
C_2	Cable diameter	0.127 mm
K_1	Inner diameter of stainless steel tube 3	1.2 mm
K_2	Outer diameter of stainless steel tube 3	1.4 mm
K_3	Inner diameter of stainless steel tube 2	1.6 mm
K_4	Outer diameter of stainless steel tube 2	1.9 mm
K_5	Inner diameter of stainless steel tube 1	2.1 mm
K_6	Outer diameter of stainless steel tube 1	2.5 mm

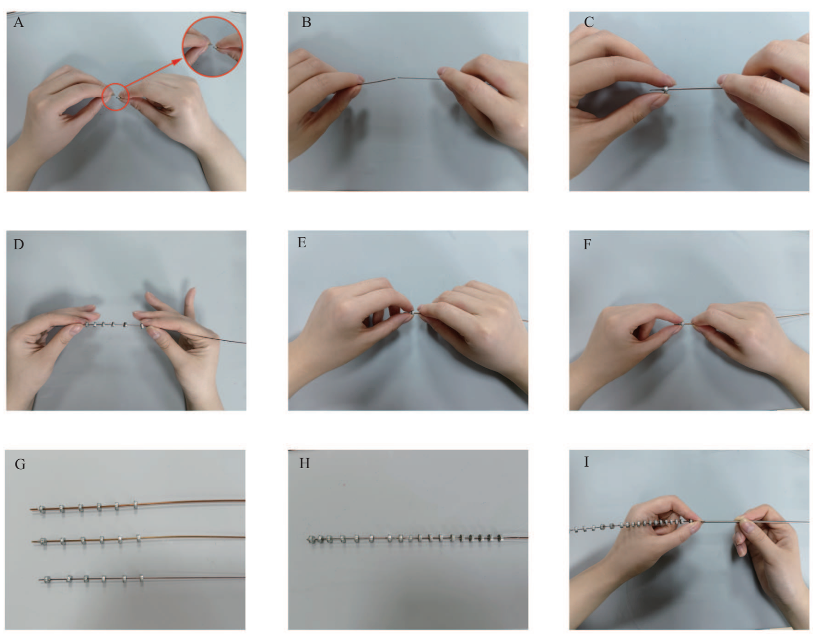

Fig. S2 Fabrication of robot body. (A) Producing all magnetic spacer disks required for a robot body. (B) Inserting elastic rod into polyimide hollow tube 3. (C) Preparing six magnetic spacer disks and sticking one to end of polyimide hollow tube 3. (D) Making remaining five magnetic spacer disks mutually exclusive on polyimide hollow tube 3. (E, F) Repeating the same steps from (C) and (D) for polyimide hollow tubes 2 and 1. (G) Obtaining all components of three-segment backbone. (H) Tying three cables to glued magnetic spacer disk in each segment, and making cables pass through subsequent magnetic spacer disks. (I) Sticking ends of three polyimide hollow tubes with three stainless steel tubes.

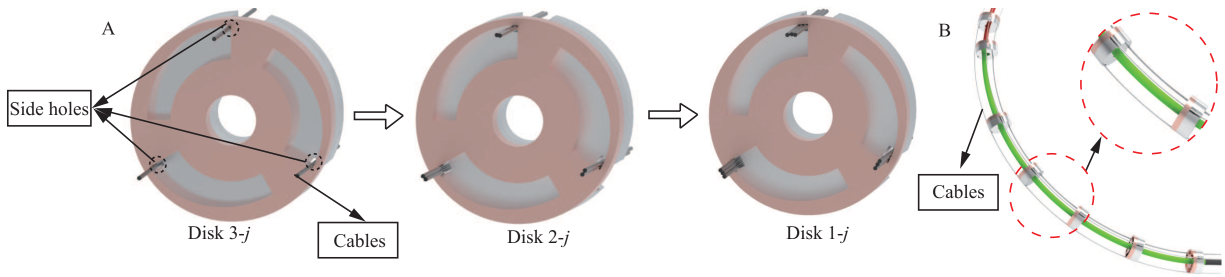

Fig. S3 Side hole configuration and cable states. (A) Side hole states with increasing cable number. (B) Cable states when backbone bends.

Table S-2 Parameters of Soft Drives

Symbol	Definition	Value
w_{B1}	Inner diameter of soft drive with large PSA	30 mm
L_{B1}	Length of soft drive with large PSA	158 mm
W_{B1}	Maximum diameter of soft drive with large PSA	64 mm
H_{B1}	Thickness of soft drive with large PSA	3 mm
w_{B2}	Inner diameter of soft drive with small PSA	10 mm
L_{B2}	Length of soft drive with small PSA	100 mm
W_{B2}	Maximum diameter of soft drive with small PSA	20 mm
H_{B2}	Thickness of soft drive with small PSA	1 mm

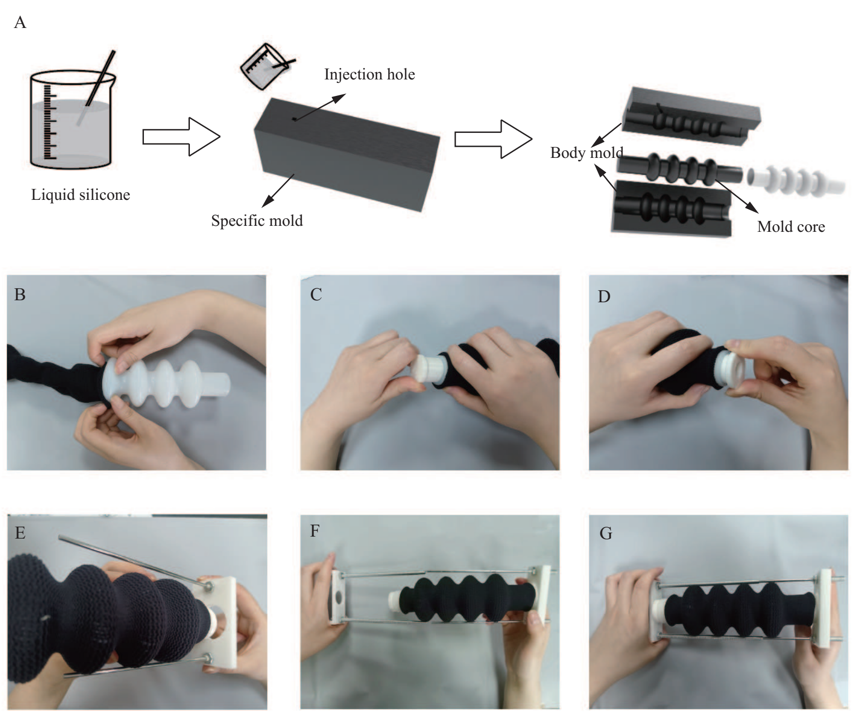

Fig. S4 Fabrication of soft drive with large PSA. (A) Obtaining a silicone tube by injection molding technology. (B) Covering silicone tube with a fiber-reinforced layer. (C, D) Inserting plug A and plug B coated with glue into both sides of silicone tube. (E) Embedding plug B in fixed side. (F) Inserting plug A into moving side. (G) Complete soft drive with large PSA.

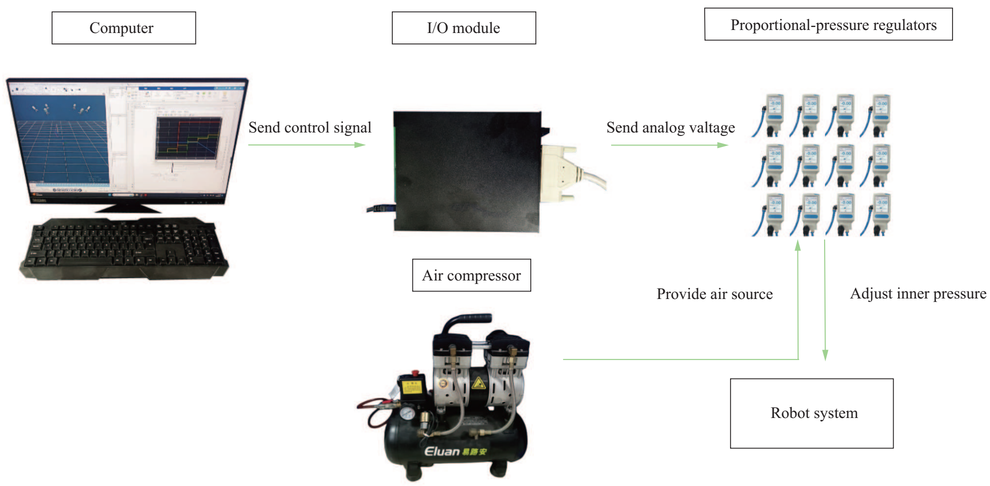

Fig. S5 Pneumatic platform.

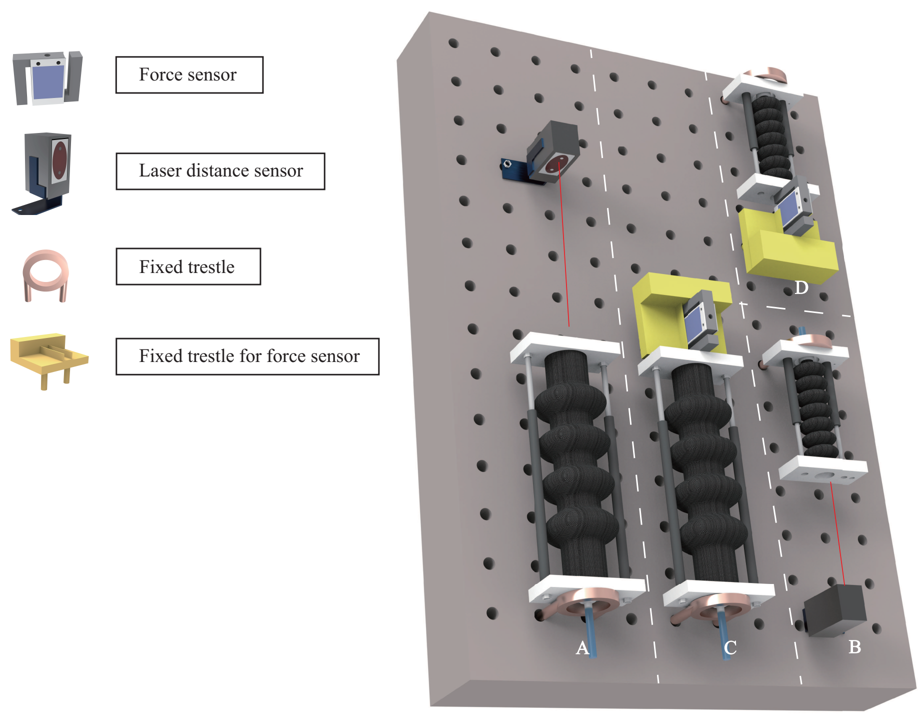

Fig. S6 Characteristic analysis platform. (A) Pressure-displacement analysis platform for soft drive with large PSA. (B) Pressure-displacement analysis platform for soft drive with small PSA. (C) Pressure-force analysis platform for soft drive with large PSA. (D) Pressure-force analysis platform for soft drive with small PSA.

action of different pressures. The laser distance sensor (Model number: HG-C1200; Manufacturer: Panasonic; Measure range: 160 mm; Accuracy: 0.2 mm) records the displacement of the moving side under different pressures. Fig. S6(C) and Fig. S6(D) are used to analyze the pressure-force characteristics for two groups of soft drives. Both sides in each group of soft drives are restricted by the fixed trestles, and one side is pressed against the force sensor (Model number: DYLY-103; Manufacturer: Daysensor; Maximum measuring force: 200 N; Accuracy: 0.06 N). Under the action of different pressures, the soft drives squeeze the force sensor. In this way, the force sensor records the output force of the soft drives at different pressures.